Journal of Pharmaceutical Research Science & Technology

journal homepage: https://ijpp.edwiserinternational.com



Original Article

Smart Delivery of a Novel Sulfur-Containing Heterocycle through a Chitosan-Stearic Acid based Polymer-Drug Conjugate: A Redox-Sensitive Strategy for Enhanced Anticancer Activity

Noushin Golzar*

Department of Chemistry, Faculty of Sciences, Persian Gulf University, Bushehr 75169, Iran

ARTICLE INFO

Received 02 September 2025 Revised 04 October 2025 Available Online 06 October 2025

Keywords:
Breast cancer therapy
Polymer–drug conjugates
Redox-responsive drug delivery
Amphiphilic chitosan derivatives
Sulfur-containing heterocycles (SHCs)

ABSTRACT

Sulfur-containing heterocycles (SHCs) have emerged as an important class of bioactive compounds with promising applications in cancer therapy, owing to their structural diversity, redox activity, and ability to interfere with multiple oncogenic pathways. However, their therapeutic potential is often limited by poor aqueous solubility, instability in circulation, and reduced efficacy against multidrug-resistant (MDR) tumors. In this study, we aimed to evaluate the anticancer activity of a novel SHC previously developed by our team and to enhance its performance through a redox-responsive nanodelivery system. Chitosan-stearic acid (CS-SA) was synthesized via EDC-mediated amidation and subsequently conjugated to SHC through a disulfide linker, yielding SHC-ss-CS-SA micelles. Structural verification by ^1H NMR confirmed successful conjugation, and UV-visible spectrophotometry determined the SHC content to be 11.3% (w/w). The amphiphilic conjugates self-assembled into stable micelles with a mean diameter of 56 nm, low polydispersity, and positive zeta potential, exhibiting a reduced critical micelle concentration compared to CS-SA alone. Redoxresponsiveness was confirmed by dithiothreitol-triggered release, where SHC-ss-CS-SA micelles displayed rapid cleavage of disulfide bonds and efficient drug liberation under intracellular-like reductive conditions, but remained stable in extracellular-like environments. Cytotoxicity assays in T47D breast cancer cells and their resistant counterpart T47D/SN150 demonstrated that SHC-ss-CS-SA micelles significantly enhanced anticancer potency compared to free SHC, reducing IC50 values and achieving a resistance reversal index of 3.62. The improved efficacy may be attributed to endocytic uptake, bypass of MRP/BCRP efflux, redoxtriggered intracellular release, and potential nuclear enrichment facilitated by chitosan's GlcNAc structure. Collectively, these findings show that SHC-ss-CS-SA micelles not only potentiate the anticancer activity of a novel sulfur-containing heterocyclic compound but also effectively overcome transporter-mediated MDR, offering a promising and safe platform for targeted cancer therapy.

This is an Open Access journal, and articles are distributed under the terms of the <u>Creative Commons Attribution 4.0 International License</u>, which permits unrestricted use, distribution, and reproduction in any medium, provided you give appropriate credit to the original author[s] and the source.

Introduction

Cancer is one of the most serious health challenges worldwide, defined by uncontrolled cell growth and the ability to invade other tissues [1]. Its global burden continues to escalate, with millions of new cases and deaths recorded annually. Despite advances in early detection and therapeutic strategies, treatment efficacy is still limited by major obstacles—drug resistance, systemic toxicity, and the ability of malignant cells to adapt through complex signaling pathways and genetic mutations [2]. These realities highlight the urgent need for innovative therapies that combine potent anticancer activity with high selectivity and reduced side effects [3-9].

Heterocyclic compounds, particularly those containing nitrogen, oxygen, or sulfur atoms in their ring systems, have proven invaluable in drug discovery [10]. They form the structural backbone of around 60% of approved anticancer agents, due to their chemical versatility, ease of modification, and broad spectrum of biological activities [11]. Benzopyrans (chromenes), belonging to the flavonoid or bioflavonoid family (derived from the Latin flavus, meaning yellow, reflecting their natural appearance), represent a class of natural molecules known for diverse pharmacological functions, including antitumor, anti-Leishmanial, and antibacterial activities [12].

These compounds interfere with cell proliferation by binding to the colchicine-binding domain of β -tubulin, thereby disrupting microtubule polymerization, halting cell cycle progression, and ultimately triggering apoptosis [13]. Importantly, chromenes have shown activity against tumor cells that exhibit resistance to conventional chemotherapeutic drugs, suggesting their potential utility in patients unresponsive to agents such as taxanes [14].

However, the precise molecular mechanisms underlying their anticancer action remain incompletely characterized, underscoring the need for further mechanistic investigations to identify more potent derivatives. Given the established role of apoptosis induction in cancer therapy, considerable efforts have been directed toward synthesizing new chromene-based analogs [15].

*Corresponding author: Noushin Golzar, Department of Chemistry, Faculty of Sciences, Persian Gulf University, Bushehr 75169, Iran.

https://doi.org/10.31531/jprst.1000197

Sulfur-containing heterocycles (SHCs) are especially noteworthy for their strong interactions with biological targets and their ability to interfere with multiple cellular pathways involved in tumor progression. However, their potential is often limited by poor water solubility, rapid systemic clearance, and nonspecific distribution—issues that nanotechnology-based delivery systems are well positioned to address [16,17].

Polymer–drug conjugates (PDCs) have emerged as a powerful platform within nanomedicine [18]. In a PDC, the drug is covalently attached to a biocompatible polymer backbone through a cleavable linker, which can be designed to respond to specific physiological or pathological stimuli [19]. This approach enhances drug stability in circulation, prolongs half-life, and enables selective release at the disease site. Linker choice is crucial: stimuli-responsive linkers exploit tumor-specific conditions such as acidic pH, enzymatic activity, or redox potential to trigger controlled release [20].

Among these stimuli, redox potential is particularly advantageous for cancer therapy. The concentration of glutathione (GSH)—a major cellular reducing agent—is substantially higher inside cells and markedly elevated in tumor cells compared to normal tissues. Disulfide bonds (–S–S–) are readily cleaved under such reductive conditions, making them ideal linkers for tumor-targeted drug delivery. Upon cellular internalization, the high GSH concentration in cancer cells can rapidly break the disulfide bond, releasing the active drug directly at its site of action [21].

glycolipid-like The copolymer chitosan oligosaccharide-g-stearic acid (CS-SA) is particularly promising carrier in this context. Synthesized by coupling the carboxyl group of stearic acid to the amino group of chitosan oligosaccharide, CS-SA is amphiphilic and can self-assemble into stable micelles in aqueous environments. These micelles exhibit excellent physicochemical stability and efficient cellular uptake, aided by hydrophobic microdomains near their surface [22-24]. However, conventional CS-SA systems often suffer from slow drug release due to the stability of amide linkages between the hydrophilic shell and hydrophobic core. Incorporating a disulfide bond as the drug-polymer linkage offers a way to overcome this limitation, enabling rapid, redoxtriggered release inside tumor cells [21].

In this study, we designed a smart redox-responsive nanosystem to deliver a novel sulfur-containing heterocyclic compound (SHC) with potent anticancer

potential. The SHC was covalently attached to CS-SA via a disulfide linker, forming micelles capable of passive tumor targeting and selective intracellular release. Once internalized into cancer cells, the elevated GSH levels cleave the disulfide bond, releasing the SHC to interact with its nuclear targets and exert its therapeutic effect. We describe the synthesis, characterization, redox-triggered release profile, and *in vitro* cytotoxicity of this SHC–ss–CS-SA system, demonstrating its promise as a platform for targeted cancer therapy.

Materials and Methods

Chitosan oligosaccharide (Mw ≈ 17.5 kDa, degree of deacetylation 95%) was obtained from Merck (Darmstadt, Germany). The sulfur-containing heterocyclic compound, 2-amino-7,7-dimethyl-5-oxo-4-(thiophen-2-yl)-5,6,7,8-tetrahydro-4H-chromene-3carbonitrile (Mw \approx 300.3754 ug/umol), was synthesized according to our previously developed method [25]. Stearic acid (SA), 1-ethyl-3-(3dimethylaminopropyl) carbodiimide dithiobis(succinimidyl propionate) (DSP), fluorescein isothiocyanate (FITC), pyrene, and dimethylthiazol-2-yl)-2,5-diphenyltetrazolium bromide (MTT) were purchased from Sigma-Aldrich (St. Louis, 1,1'-Dioctadecyl-3,3,3',3'-USA). tetramethylindotricarbocyanine iodide (DiR) was obtained from Sigma-Aldrich. Dulbecco's modified Eagle's medium (DMEM), fetal bovine serum (FBS), and trypsin-EDTA were sourced from Merck.

Synthesis of CS-SA

The chitosan oligosaccharide-stearic acid (CS-SA) conjugate was prepared through a single-step amidation reaction, following established protocols with slight modifications [26]. In brief, 1.0 g of CS (Mw ≈ 17.5 kDa) was dissolved in 60 mL of deionized water. Separately, 1.65 g of stearic acid (SA) and 11.0 g of 1ethyl-3-(3-dimethylaminopropyl) carbodiimide (EDC) were dissolved in ethanol and pre-activated at 60 °C for 30 min to promote coupling. The activated ethanol solution was then added dropwise to the CS solution under continuous stirring and maintained at 80 °C for 4 h. The resulting mixture was subjected to dialysis against deionized water using a membrane with a molecular weight cut-off (MWCO) of 7000 Da for 48 h, followed by freeze-drying. The lyophilized product was washed with ethanol to remove any residual reagents, redispersed in deionized water, and freeze-dried again to yield the final CS-SA conjugate.

Synthesis of SHC-Conjugated CS-SA (SHC-SS-CS-SA)

The conjugation of SHC to CS–SA micelles through a disulfide linkage using dithiobis(succinimidyl propionate) (DSP) was carried out in two sequential steps, with all reactions protected from light [19,21]. Initially, SHC and DSP were separately dissolved in DMSO, each at 20 mg/mL. The SHC solution was slowly added dropwise to the DSP solution at a 1:1 molar ratio, followed by the addition of a catalytic amount of triethylamine (0.5 μ L). The mixture was stirred at room temperature for 2 h, dialyzed against deionized water (MWCO 3000 Da) for 24 h, and freezedried to yield the SHC–DSP intermediate.

In the second step, CS-SA was dispersed in deionized water with ultrasonic assistance to form a uniform micelle solution, and the pH was adjusted to 7.4. The SHC-DSP intermediate was dissolved in DMSO (10 mg/mL) and added dropwise to the CS-SA micelle dispersion at a SHC:CS-SA weight ratio of 1:10. The reaction mixture was stirred for 12 h at room temperature, dialyzed against deionized water (MWCO 7000 Da) for 48 h, and freeze-dried. The resulting solid was washed three times with DMSO to remove unreacted SHC-DSP, redissolved in water, and lyophilized again to obtain the final SHC-SS-CS-SA conjugate.

Physicochemical Characterization of products

¹H NMR Spectroscopy

Proton nuclear magnetic resonance (¹H NMR) spectroscopy was employed to confirm the chemical structures of the synthesized compounds. Samples were prepared at a concentration of 20.0 mg/mL and dissolved in either dimethyl sulfoxide-d6 (DMSO-d6) or deuterium oxide (D2O) prior to analysis.

Determination of SA Content in CS-SA

The stearic acid (SA) content of the CS–SA conjugate was quantified using the 2,4,6-trinitrobenzenesulfonic acid (TNBS) assay. Briefly, 0.3 mL of CS–SA solution (1 mg/mL) was mixed with 2.0 mL of 4.0% NaHCO₃ and 2.0 mL of 0.1% TNBS solution, followed by incubation at 37 °C for 2 h. The reaction was then stopped by adding 2.0 mL of 2 mol/L HCl. The absorbance was measured at 344 nm using a UV–visible spectrophotometer. The degree of SA substitution in CS–SA was calculated using the following equation [26]:

$$\frac{A_{CS}}{A_{CS-SA}} = \frac{M_{CS-SA}}{M_{CS}} \times \frac{n_{NH2}}{n_{NH2} - m_{NH2}}$$

Where, A_{CS} is the UV absorbance of CS, A_{CS-SA} is the UV absorbance of CS–SA, M_{CS-SA} and M_{CS} are the molecular weights of CS–SA and CS, respectively, n_{NH2} is the total moles of amino groups in the CS chain, and m_{NH2} is the molar amount of SA bound to CS.

SHC Content in SHC-SS-CS-SA

The amount of SHC incorporated into the SHC–SS–CS–SA conjugate was determined using a UV–visible spectrophotometer (DU640, Beckman-Coulter, USA) [27]. Samples of free SHC and SHC–ss–CS–SA were each dispersed in a dimethyl sulfoxide/deionized water mixture (5:95, v/v). The SHC content in the conjugate was quantified by comparison to a calibration curve prepared from standard SHC solutions.

Critical Micelle Concentration (CMC)

The CMC of SHC–ss–CS–SA micelles was determined using pyrene as a hydrophobic fluorescent probe. The fluorescence intensity ratio (I_1/I_3) was calculated from the first peak at 374 nm (I_1) and the third peak at 385 nm (I_3) in the pyrene emission spectra. Micellar solutions at varying concentrations were prepared with a fixed pyrene concentration of 5.93×10^{-7} mol/L and excited at 337 nm. Emission spectra were recorded over the range of 360–450 nm using a fluorescence spectrophotometer (F-2500, Hitachi Co., Japan). Excitation and emission slit widths were set to 10.0 nm and 2.5 nm, respectively [28].

Particle Size and Zeta Potential

Micelle size distribution was analyzed by dynamic light scattering (DLS) on a Zetasizer instrument (Malvern Instruments Ltd., UK). The same instrument was used to determine the zeta potential of the micelles [29].

Particle Morphology

Micelle morphology was visualized by transmission electron microscopy (TEM, JEOL JEM-1230, Japan). Samples were deposited on carbon-coated copper grids, negatively stained with 2% (w/v) phosphotungstic acid, and air-dried before observation [29].

Redox-Responsive Behavior and In Vitro SHC Release

To confirm the redox sensitivity of the disulfide linkage and assess the release of SHC under reductive conditions, SHC–SS–CS–SA micelles were dispersed in phosphate-buffered saline (PBS, pH 7.4) containing either 10 mM or 10 μ M dithiothreitol (DTT), with a final drug concentration of 5 μ g/mL. Fluorescence intensity was recorded at predetermined intervals (0–50 min) using a fluorescence spectrophotometer, with an excitation wavelength of 505 nm. As a control, fluorescence from free SHC at the same concentration was measured under identical conditions [19].

The in vitro drug release profile was studied by a dialysis method in PBS (pH 7.4) supplemented with either 10 mM or 10 µM DTT. Micelles containing an equivalent of 100 µg of SHC were placed in dialysis bags (MWCO 7000 Da) and immersed in 20 mL of the release medium. At specified time points, aliquots of the external medium were collected and replaced with fresh buffer. SHC concentrations were quantified fluorometrically (Ex = 505 nm, Em = 565 nm) against a standard calibration curve. Free SHC release was evaluated in parallel under the same experimental setup. All measurements were performed in triplicate [30].

Cell Culture

Human breast cancer T47D cells and their multidrugresistant variant, T47D/SN150, were purchased from Royan institute. All cell lines were maintained in Dulbecco's modified Eagle's medium (DMEM) supplemented with 10% (v/v) fetal bovine serum (FBS) and incubated in a humidified environment containing 5% CO₂ at 37 °C. Subculturing was routinely carried out using trypsin—ethylenediaminetetraacetic acid (EDTA) solution [31].

In Vitro Antitumor Activity

The cytotoxic potential of SHC, SHC–ss–CS–SA micelles, and CS–SA against T47D, and T47D/SN120 cells was evaluated using the MTT assay. Cells were seeded into 96-well plates at a density of 1.0×10^4 cells per well and allowed to adhere for 24 h. Following this, cells were treated with varying concentrations of SHC, CS–SA, or SHC–ss–CS–SA micelles and incubated for an additional 48 h. Subsequently, 20 μL of MTT solution (5 mg/mL) was added to each well, and the plates were incubated for 4 h at 37 °C. After removing the medium, 200 μL of DMSO was added to dissolve the formazan crystals formed. Absorbance was measured at 570 nm using a microplate reader (Model 680, Bio-Rad, USA). All assays were conducted in triplicate [32].

The ability of SHC-SS-CS-SA micelles to overcome drug resistance was calculated according to the following formula:

$$OP = \frac{(R_f/R_m)}{(S_f/S_m)}$$

Where: OP is overcome power, $R_f = IC_{50}$ of free SHC in resistant cells, $R_m = IC_{50}$ of SHC–ss–CS–SA in resistant cells, $S_f = IC_{50}$ of free SHC in sensitive cells, and $S_m = IC_{50}$ of SHC–ss–CS–SA in sensitive cells [33].

Statistical Analysis

All results are expressed as mean \pm standard deviation (SD) from independent experiments. Comparisons between two groups were conducted using a two-tailed Student's t-test, with p < 0.05 considered statistically significant. For multiple group comparisons, one-way analysis of variance (ANOVA) followed by Tukey–Kramer post hoc testing was applied. Differences were regarded as statistically significant when the p-value was below 0.05 [32].

Results

Synthesis of CS-SA and SHC-SS-CS-SA

The CS-SA conjugate was obtained through an EDCmediated amidation between the amino groups of CS and the carboxyl group of stearic acid (SA). The degree of SA substitution on CS was determined to be 14.61% (molar ratio). Subsequently, SHC-ss-CS-SA was synthesized using DSP as the redox-cleavable linker. Figure 1 illustrates the synthetic route for SHC-DSP, CS-SA and SHC-ss-CS-SA. Structural verification of the products was performed using ¹H NMR spectroscopy (Figure 2). In the ¹H NMR spectrum of SHC-DSP, peaks at around 1 ppm were assigned to the methyl protons of the SHC moiety, while signals near 2.8 ppm corresponded to the protons of the Nhydroxysuccinimide (NHS) group from DSP. For CS-SA, peaks at approximately 0.9 and 1.1 ppm were attributed to the methyl (-CH₃) and methylene (-CH₂-) groups of SA, respectively. In the ¹H NMR spectrum of SHC-ss-CS-SA, the methyl peaks of SHC around 1 ppm were still observed but overlapped with the -CH₃ and -CH2- signals of SA, while additional minor aromatic proton signals from SHC emerged near 7.2 ppm, collectively confirming the successful conjugation. The SHC content in SHC-ss-CS-SA, measured by UV-visible spectrophotometry, was found to be 11.3% (w/w).

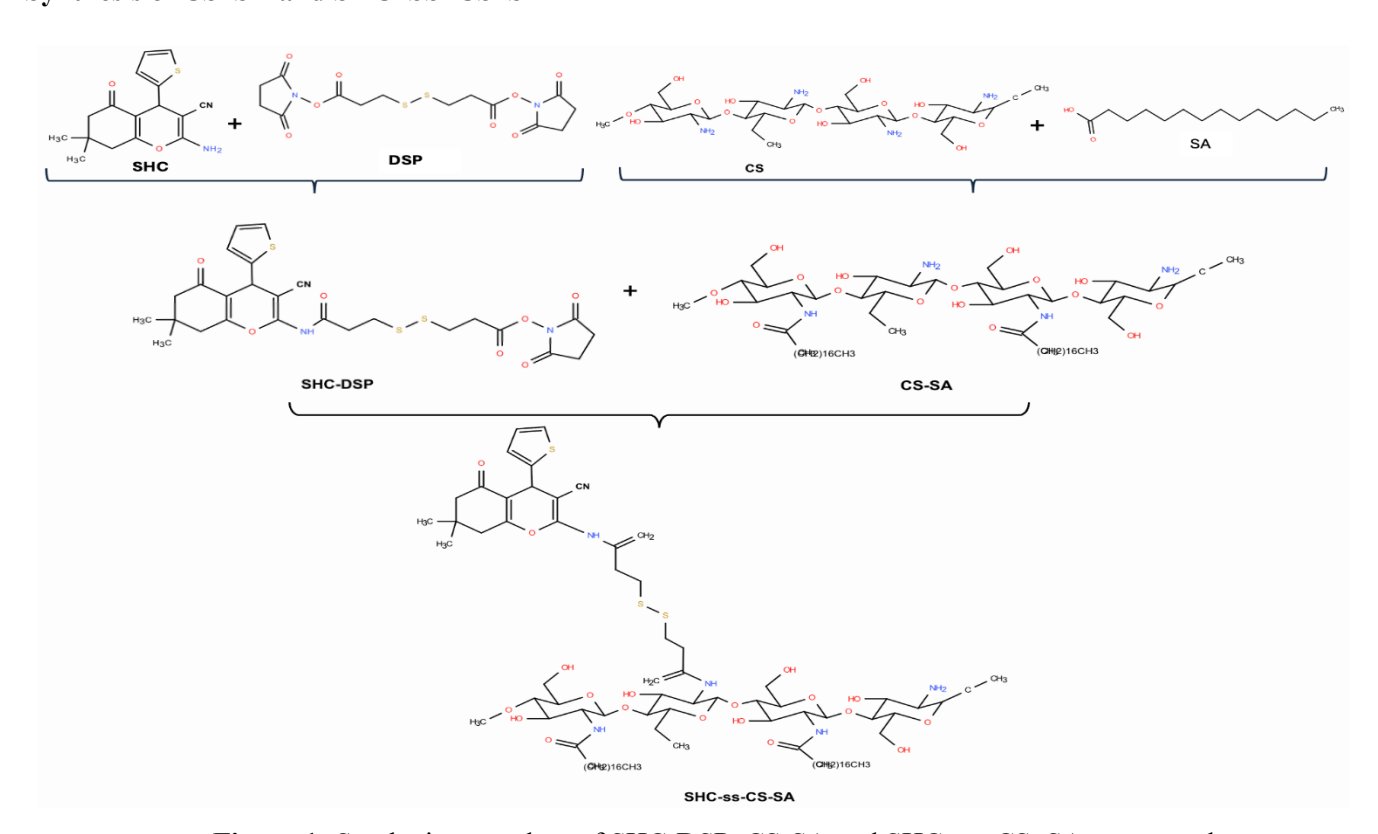


Figure 1: Synthetic procedure of SHC-DSP, CS-SA and SHC-ss-CS-SA compounds.

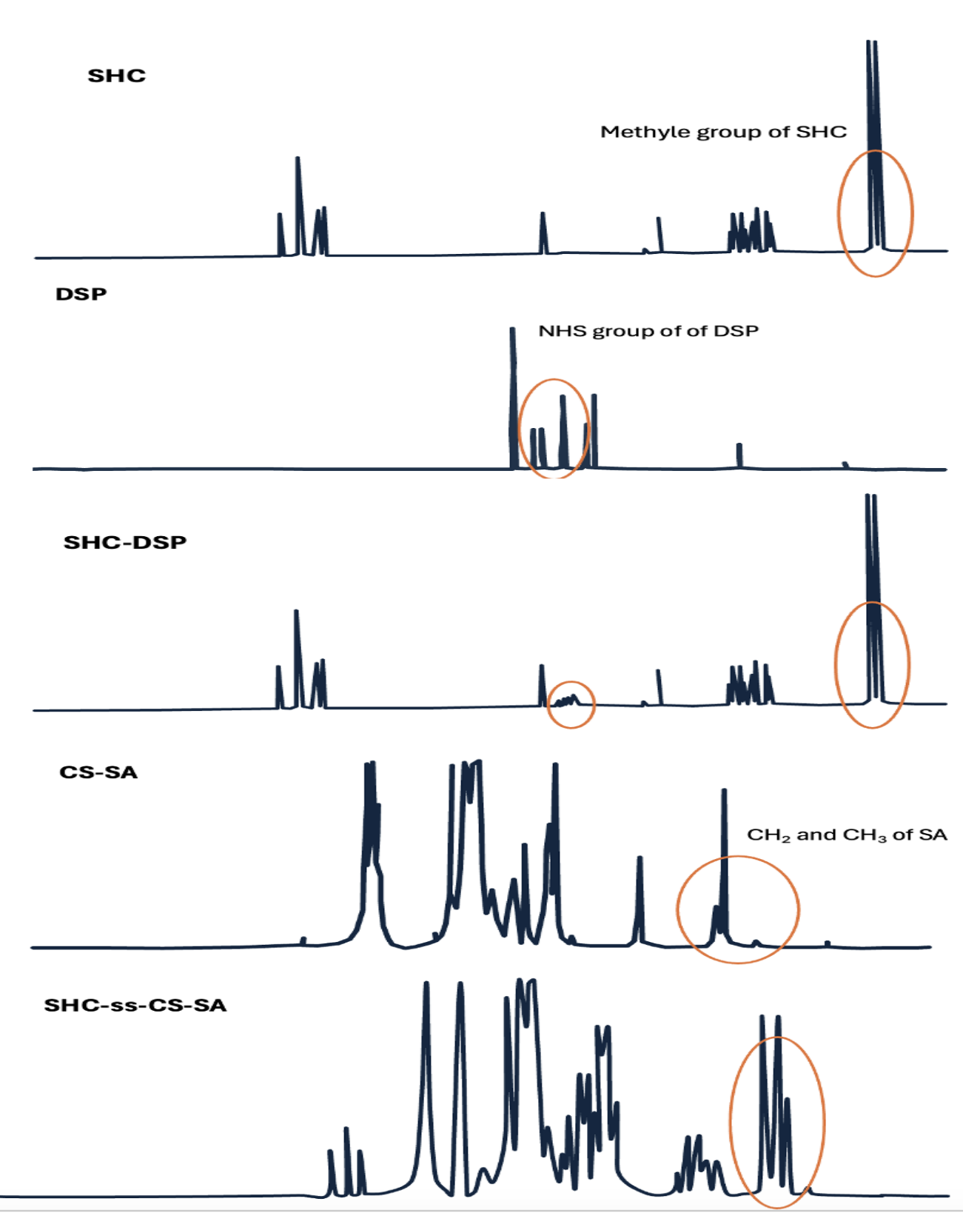


Figure 2: ¹H NMR spectra of SHC, DSP, SHC-DSP, CS-SA and SHC-ss-CS-SA.

Physicochemical Characteristics of SHC-ss-CS-SA

The synthesized SHC-ss-CS-SA conjugate readily self-assembled into micelles in aqueous solution, driven by the amphiphilic nature of the molecule—hydrophilic

CS chains linked to hydrophobic moieties from SA and SHC. Table 1 summarizes the key physicochemical properties of SHC-ss-CS-SA. The critical micelle concentration (CMC) measurement confirmed the self-aggregation capacity of both CS-SA and SHC-ss-CS-SA.

Table 1: Physico-chemical characteristics of micelle-like nanoparticles.

Sample	CMC (µg/mL)	Size (nm)	PDI	Zeta potential (mV)
CS-SA NPs	56.69	45.5 ± 5.8	0.202 ± 0.005	34.01 ± 1.4
SHC-ss-CS-SA NPs	45.83	56.15 ± 3.3	0.237 ± 0.008	20.76 ± 2.1

As illustrated in Figure 3a, the fluorescence intensity ratio between the first and third peaks (I_1/I_3) of pyrene emission remained stable at approximately 1.6 when the concentration was low. However, once the critical micelle concentration (CMC) was reached, the I_1/I_3 ratio decreased abruptly, signifying the entrapment of pyrene within the hydrophobic cores of the micelles. The CMC values determined in PBS were about 56.69 μ g/mL for CS–SA and 45.83 μ g/mL for SHC–ss–CS–SA, demonstrating that SHC conjugation improved the dispersity and micellization efficiency of CS–SA in aqueous buffers.

Size distribution data, zeta potential measurements, and Transmission electron microscopy (TEM) images, for CS–SA and SHC–ss–CS–SA micelles are shown in Figures 3b-e and Table 1. DLS revealed that SHC–ss–CS–SA micelles were larger in diameter (56.15 ± 3.3 nm) compared to CS–SA micelles (45.5 ± 5.8 nm), consistent with the TEM measurements. Furthermore, SHC–ss–CS–SA micelles exhibited a lower positive zeta potential (20.76 ± 2.1 mV) than CS–SA micelles (34.01 ± 1.4 mV), likely due to the reduced number of free amine groups on the micelle surface and the increase in micelle size following SHC conjugation.

In Vitro Redox-Responsive Release of SHC

To evaluate the sensitivity of SHC-ss-CS-SA micelles to reductive conditions, their fluorescence emission was monitored over time in the presence of dithiothreitol (DTT). It was found out that fluorescence of SHC is

quenched when covalently linked to a polymer backbone but is restored upon release from the polymer. DTT concentrations of 10 mM and 10 μ M were selected to mimic intracellular and extracellular thiol levels, respectively.

As shown in Figure 4a, when incubated in PBS (pH 7.4) containing 10 mM DTT, the fluorescence intensity of SHC–ss–CS–SA micelles increased steadily and reached a plateau comparable to free SHC within 60 min, indicating cleavage of the disulfide bonds and liberation of SHC from the carrier. Quantitative analysis (Figure 4b) confirmed that the disulfide bonds were rapidly cleaved within 30 min under strongly reductive conditions but remained stable for at least 60 min in a weakly reductive environment (p < 0.05).

The *in vitro* release profiles in different media are presented in Figure 4c. As expected, free SHC exhibited complete release within 48 h. Under conditions simulating extracellular thiol levels (10 μ M DTT), SHC–ss–CS–SA micelles released approximately 28.12% of their SHC content within 48 h. In contrast, at 10 mM DTT, mimicking the intracellular environment, cumulative release reached ~87.08% over the same period. The release rate at 10 mM DTT was significantly higher than at 10 μ M DTT (p < 0.05). These findings indicate that SHC–ss–CS–SA micelles are stable in nonreducing environments yet respond rapidly to intracellular-like reductive conditions, enabling efficient drug release.

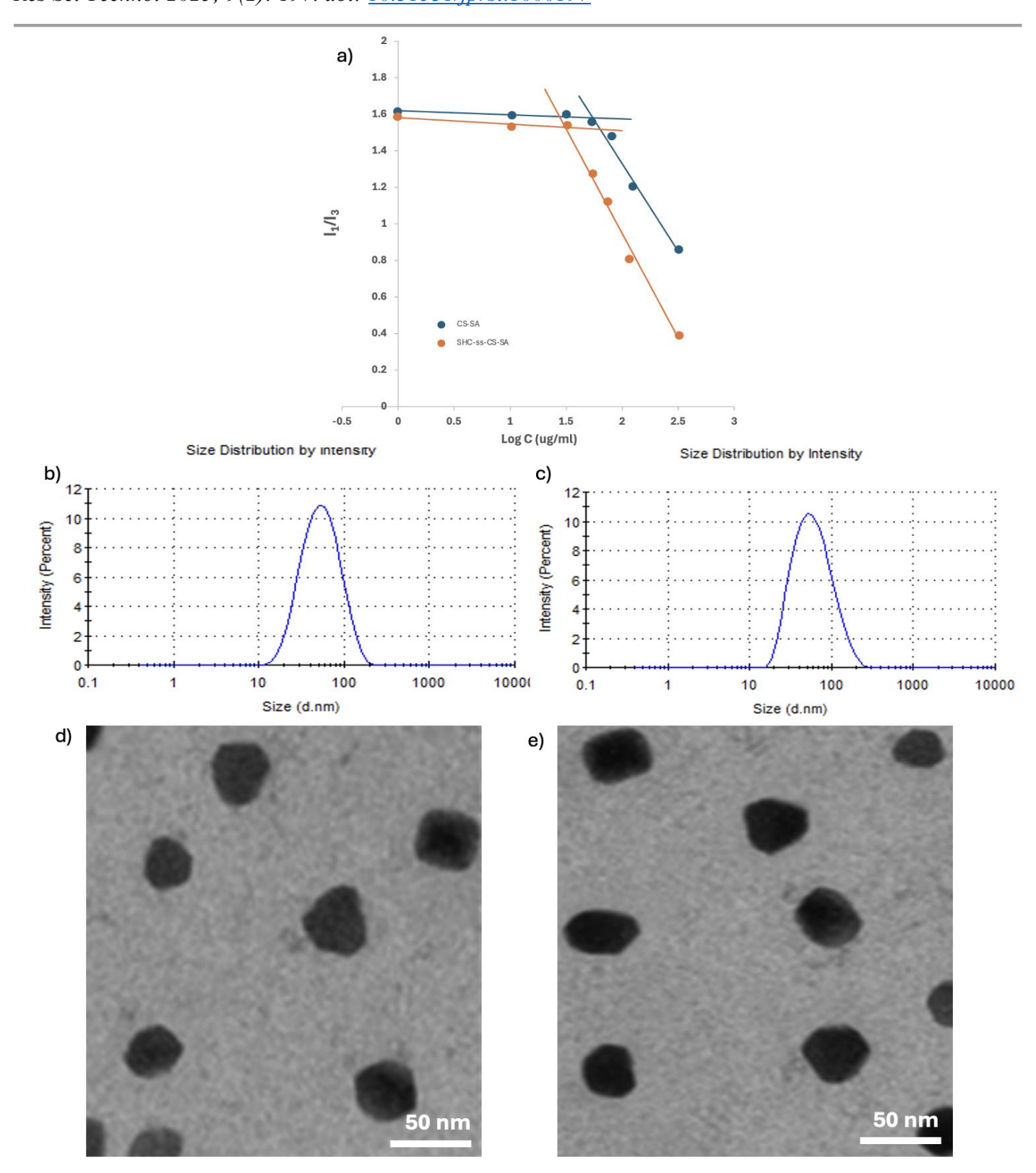


Figure 3: (a) Fluorescence intensity ratio (I₁/I₃) as a function of logarithmic concentration for CS-SA and SHC-ss-CS-SA; Particle size distribution of b) CS-SA and c) SHC-ss-CS-SA nanoparticles, and TEM images of d0 CS-SA and e) SHC-ss-CS-SA nanoparticles.

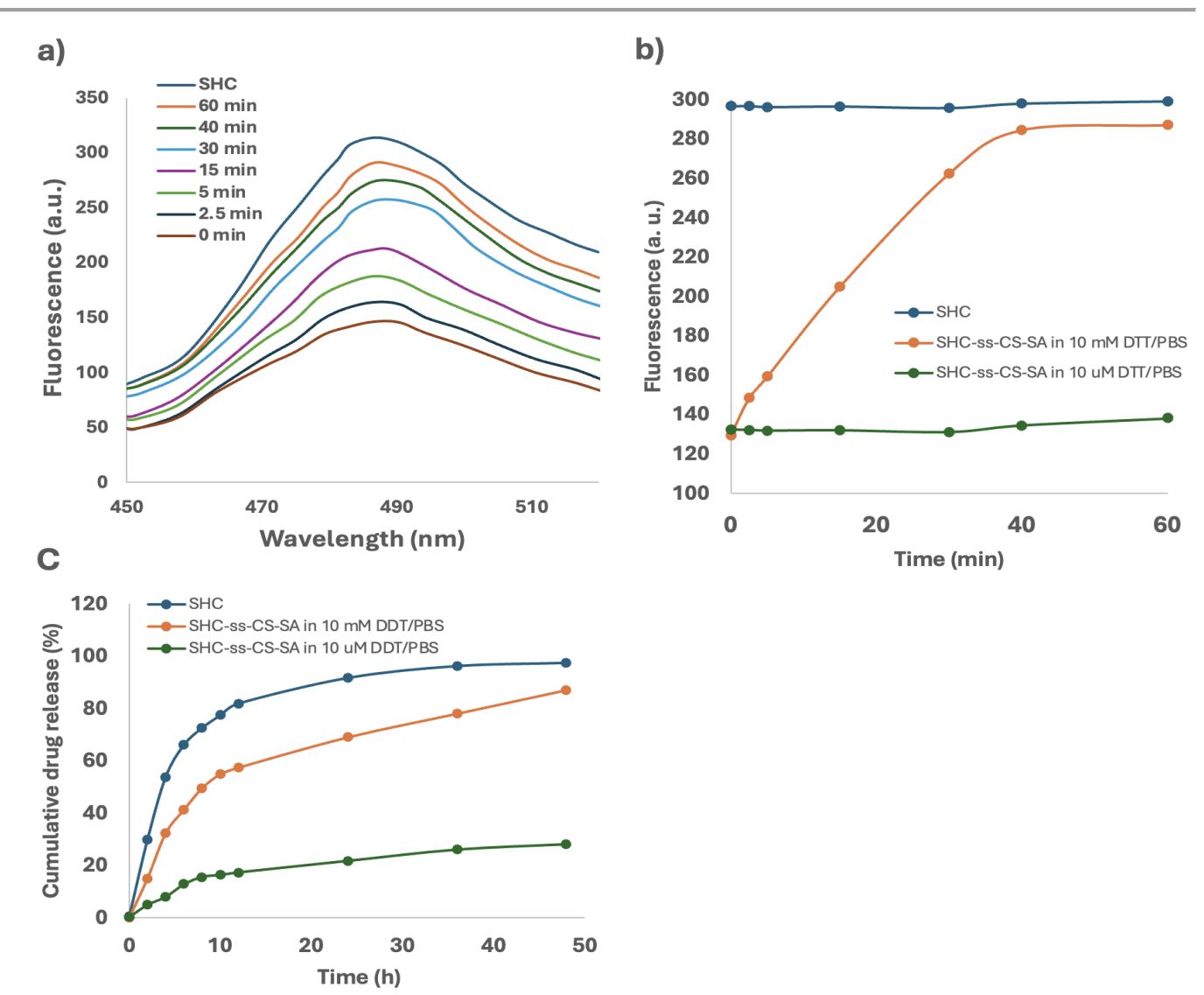


Figure 4: Redox sensitivity and *in vitro* drug release from DOX-SS-CSO-SA micelles. (a) Fluorescence emission spectra of SHC-ss-CS-SA micelles incubated in PBS (pH 7.4) with 10 mM DTT at various time intervals. (b) Fluorescence intensity changes and (D) SHC release profiles under different conditions: SHC-ss-CS-SA in PBS with 10 mM DTT, SHC-ss-CS-SA in PBS with 10 mM DTT.

In Vitro Cytotoxicity

The cytotoxic potential of SHC-ss-CS-SA micelles was evaluated in T47D, and T47D/SN150, cell lines,

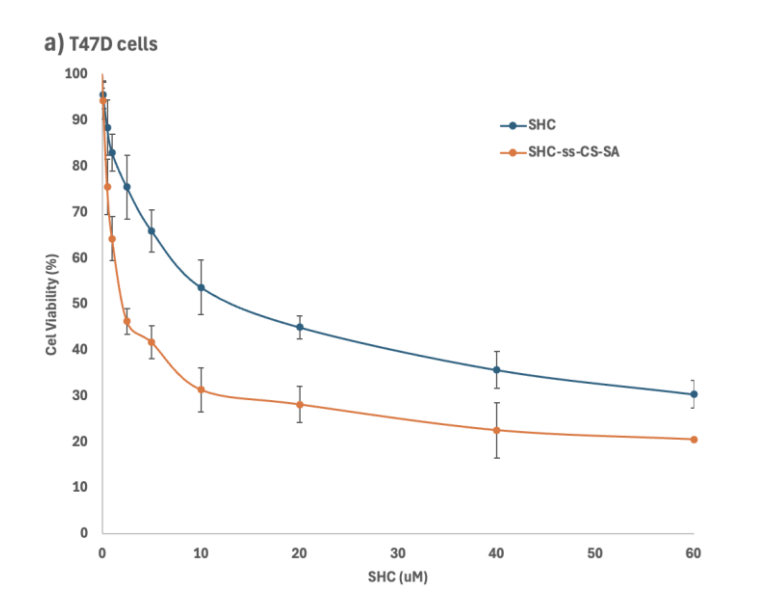
with free SHC used as controls. Previous studies have indicated that conjugating chemotherapeutic drugs via a short amine linker does not diminish its anticancer potency [28,29]. The 50% inhibitory concentration (IC₅₀) values for T47D, and T47D/SN50 cells were determined using the MTT assay (Table 2).

Table 2: Cytotoxicity (IC₅₀) of CS-SA, free SHC, and SHC-ss-CS-SA nanoparticles against T47D, and T47D/SN150 cells.

Sample code	T47D	T47D/SN120	Overcome power
CS-SA	361 ± 17	512 ± 27	-
SHC	6.64 ± 1.30	74.80 ± 9.11	-
SHC-ss-CS-SA	3.77 ± 0.51	11.71 ± 0.86	3.62

As presented in Table 1, CS–SA micelles displayed relatively low toxicity, with IC₅₀ values of approximately 361, and 512 μ g/mL for T47D, and T47D/SN150 cells, respectively. In T47D cells, SHC–ss–CS–SA micelles achieved significantly lower IC₅₀ value than free SHC (p < 0.05), and cell viability decreased progressively with increasing micelle concentration (Figure 5 a,b).

In T47D/SN150 cells, the IC₅₀ of SHC was 11.7-fold higher than that observed in T47D cells, confirming the strong drug resistance of this line. However, for SHC–ss–CS–SA micelles, the IC₅₀ difference between T47D/SN150 and T47D cells was only 3.1-fold, yielding a drug resistance reversal index of 3.62. These data demonstrate the ability of SHC–ss–CS–SA micelles to effectively overcome multidrug resistance (MDR) in T47D/SN150 cells (Table 2).



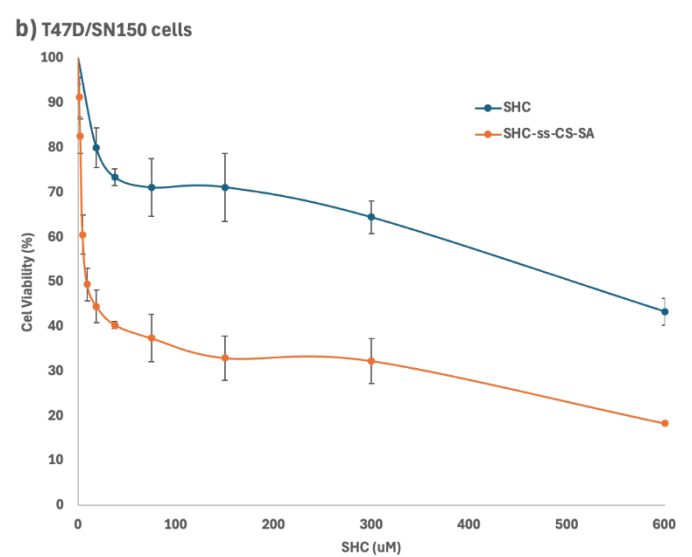


Figure 5: Dose-dependent cytotoxicity of free SHC, and SHC–ss–CS–SA nanoparticles against T47D, and T47D/SN150.

Discussion

SHC-ss-CS-SA micelles were prepared via an amidation reaction between the N-hydroxysuccinimide (NHS) ester groups of DSP-SHC and the amino groups of CS-SA micelles under physiological pH and room temperature, forming stable amide linkages [19,21,26]. Through this approach, SHC was covalently anchored to the CS-SA backbone via redox-sensitive disulfide bonds. The resulting polymer-drug conjugates retained the amphiphilic nature of the polymer carrier, enabling spontaneous self-assembly into core-shell micelles in aqueous solution, thereby improving the aqueous solubility of the hydrophobic SHC.

In the H₂O/DMSO reaction system, the amino groups of CS are predominantly located on the micelle surface [26]. Based on collision theory, when SHC–DSP solution was gradually introduced into the CS–SA dispersion, the activated succinyl groups of SHC–DSP preferentially reacted with these surface amino groups. As a result, part of the hydrophobic SHC was likely displayed at or near the micelle exterior. This

configuration was supported by the observed increase in micelle size and the reduction in zeta potential compared with CS-SA alone (Table 1). Importantly, this structure facilitated rapid SHC release in reductive environments.

The disulfide linkage in SHC-ss-CS-SA served as a redox-cleavable trigger for intracellular drug release [19,21]. Under high intracellular thiol concentrations—mimicked by 10 mM DTT—the disulfide bonds were efficiently cleaved, liberating SHC from the carrier and allowing its transport into the nucleus (Figure 4). Conversely, in extracellular fluids or systemic circulation, where thiol concentrations are markedly lower, negligible drug leakage occurred. Additionally, the nanoscale size and amphiphilic architecture of the micelles allow passive accumulation at tumor sites via the enhanced permeability and retention (EPR) effect, while reducing off-target distribution—especially to the heart—thereby potentially minimizing drug-induced cardiotoxicity [32,34].

Multidrug resistance in tumor cells is frequently associated with the overexpression of efflux transporters such as MRP and BCRP, which actively reduce intracellular drug accumulation [31]. In resistant T47D/SN150 cells, free SHC was readily eliminated by these transporters, resulting in diminished cytotoxic activity. By contrast, SHC–ss–CS–SA micelles were taken up primarily through endocytic pathways, allowing efficient intracellular delivery and bypassing efflux-mediated clearance [32,34]. This redoxresponsive micellar system therefore provided a sustained release of SHC within the cytoplasm, leading to markedly improved cytotoxic effects in resistant cells and demonstrating its potential to overcome transporter-driven multidrug resistance (Figure 5) [19,21].

SHC-ss-CS-SA micelles, owing to the cationic nature and structural characteristics of the CS-SA backbone, are predominantly internalized through endocytosis rather than passive diffusion [34]. This uptake route facilitates sustained intracellular retention of SHC and circumvents efflux mediated by MRP and BCRP at the plasma membrane. Moreover, since efflux pumps such as P-gp and MRPs (e.g., MRP1, MRP4) are ATP-dependent, reliance on endocytic entry may further mitigate transporter activity by limiting ATP availability, thereby enhancing the capacity of the micelles to overcome multidrug resistance [31, 34].

Interestingly, earlier studies have shown that proteins containing O-linked N-acetylglucosamine (GlcNAc) are abundant in the cytoplasmic and nucleoplasmic regions of nuclear membranes [35]. Given that the monomer unit of chitosan is structurally identical to GlcNAc, CS–SA may possess a natural affinity for nuclear localization [36]. Since SHC potentially exerts its anticancer effects through nuclear targets, this potential nuclear enrichment could enhance its therapeutic potency. Collectively, these attributes explain the strong ability of SHC–ss–CS–SA micelles to overcome multidrug resistance in T47D/SN150 cells (Table 2 and Figure 5).

Conclusion

The primary objective of this study was to investigate the anticancer activity of a novel sulfur-containing heterocyclic compound (SHC) that had been previously developed by our team, and to evaluate whether its therapeutic potential could be further enhanced through the design of a nanodelivery system. To achieve this, SHC was covalently conjugated to CS–SA through a redox-cleavable disulfide linkage, yielding a polymer—

drug conjugate (SHC-ss-CS-SA) with multiple advantages for tumor-targeted therapy.

First, the incorporation of SHC into the polymeric carrier significantly improved its aqueous solubility and stability compared to the free compound, thereby enhancing its bioavailability and potential for systemic administration. Second, the amphiphilic nature of the CS–SA backbone enabled self-assembly into stable micelles with a low critical micelle concentration, providing a favorable platform for passive tumor targeting via the enhanced permeability and retention (EPR) effect. Third, the disulfide linkage endowed the system with a redox-responsive release mechanism: while remaining stable in the circulation, the conjugate was rapidly cleaved in the highly reductive intracellular environment of tumor cells, ensuring selective and timely release of active SHC within the target site.

the SHC-ss-CS-SA Importantly, nanosystem demonstrated the ability to reduce the drug resistance of T47D/SN150 cells compared with free SHC. While the precise mechanism was not directly examined in this study, the improved cytotoxicity and MDR reversal could be attributed to several contributing factors. These include the potential for endocytic uptake of the cationic micelles, which may bypass efflux recognition by MRP and BCRP transporters; enhanced intracellular retention due to micelle-mediated delivery; and redox-triggered release of SHC in the cytosolic environment, which would facilitate efficient drug activation within resistant cells. Together, these effects may underlie the reduced resistance index observed for the micellar formulation compared to the free drug.

Overall, the therapeutic outcome of SHC-ss-CS-SA reflected the synergistic benefits of this smart nanodelivery system: improved solubility and stability, passive endocytic uptake, redox-triggered intracellular release, a potential ability to evade efflux-mediated MDR, and potentially reduced systemic toxicity. Taken together, these findings highlight that conjugating SHC into a redox-responsive polymeric micelle system is not only an effective strategy to enhance the anticancer potential of this novel sulfur-containing heterocyclic compound but also establishes SHC-ss-CS-SA as a promising and safe nanoplatform for future targeted cancer therapy.

It should be noted, however, that this study did not directly monitor cellular uptake pathways or quantify intracellular SHC distribution, and thus the mechanistic explanations for MDR reversal remain hypothetical. Future studies using uptake assays, transporter

inhibition experiments, and live-cell imaging will be necessary to confirm these proposed mechanisms and further optimize the nano-delivery system.

Funding

No financial assistance was provided for this project.

Conflict of Interest

None declared.

Author Contributions

All the authors contributed to the study.

References

- Saini, Anupam, Manish Kumar, Shailendra Bhatt, Vipin Saini, and Anuj Malik. "Cancer causes and treatments." Int J Pharm Sci Res 11, no. 7 (2020): 3121-3134.
- 2. Singh, Arpita, and S. Roghini. "Cancer: Unraveling the Complexities of Uncontrolled Growth and Metastasis." PEXACY International Journal of Pharmaceutical Science 2, no. 8 (2023): 59-73.
- 3. Jin, Haojie, Liqin Wang, and René Bernards. "Rational combinations of targeted cancer therapies: background, advances and challenges." Nature Reviews Drug Discovery 22, no. 3 (2023): 213-234.
- 4. Baghbani, Fatemeh, Fathollah Moztarzadeh, Jamshid Aghazadeh Mohandesi, Fatemeh Yazdian, and Manijhe Mokhtari-Dizaji. "Novel alginate-stabilized doxorubicin-loaded nanodroplets for ultrasounic theranosis of breast cancer." International journal of biological macromolecules 93 (2016): 512-519.
- Cavanagh, Robert J., Patrícia F. Monteiro, Cara Moloney, Alessandra Travanut, Fatemeh Mehradnia, Vincenzo Taresco, Ruman Rahman et al. "Free drug and ROS-responsive nanoparticle delivery of synergistic doxorubicin and olaparib combinations to triple negative breast cancer models." Biomaterials Science 12, no. 7 (2024): 1822-1840.
- 6. Samani, Roghayeh Kamran, Fatemeh Maghsoudinia, Fatemeh Mehradnia, Seyed Hossein Hejazi, Mohsen Saeb, Tayebe Sobhani, Zohreh Farahbakhsh, Masoud A. Mehrgardi, and Mohamad Bagher Tavakoli. "Ultrasound-guided chemoradiotherapy of breast cancer using smart methotrexate-loaded perfluorohexane nanodroplets." Nanomedicine: Nanotechnology, Biology and Medicine 48 (2023): 102643.

- 7. Maghsoudinia, Fatemeh, Mohamad Bagher Tavakoli, Roghayeh Kamran Samani, Seyed Hossein Hejazi, Tayebe Sobhani, Fatemeh Mehradnia, and Masoud A. Mehrgardi. "Folic acid-functionalized gadolinium-loaded phase transition nanodroplets for dual-modal ultrasound/magnetic resonance imaging of hepatocellular carcinoma." Talanta 228 (2021): 122245.
- 8. Givarian, Mahshid, Fathollah Moztarzadeh, Maryam Ghaffari, AmirHossein Bahmanpour, Maryam Mollazadeh-Bajestani, Manijhe Mokhtari-Dizaji, and Fatemeh Mehradnia. "Dual-trigger release of berberine chloride from core-shell gelatin/perfluorohexane structure." Bulletin of the National Research Centre 48, no. 1 (2024): 65.
- 9. Samani, Roghayeh Kamran, Masoud A. Mehrgardi, Fatemeh Maghsoudinia, Mohammad Najafi, and Fatemeh Mehradnia. "Evaluation of folic acid-targeted gadolinium-loaded perfluorohexane nanodroplets on the megavoltage X-ray treatment efficiency of liver cancer." European Journal of Pharmaceutical Sciences 209 (2025): 107059.
- Taylor, Alexandria P., Ralph P. Robinson, Yvette M. Fobian, David C. Blakemore, Lyn H. Jones, and Olugbeminiyi Fadeyi. "Modern advances in heterocyclic chemistry in drug discovery." Organic & biomolecular chemistry 14, no. 28 (2016): 6611-6637.
- 11. Jahangir MA, Imam SS, Muheem A, Chettupalli A, Al-Abbasi FA, Nadeem MS, Kazmi I, Afzal M, Alshehri S. Nanocrystals: Characterization overview, applications in drug delivery, and their toxicity concerns. Journal of Pharmaceutical Innovation. 2022 Mar;17(1):237-48.
- 12. Pratap, Ramendra, and Vishnu Ji Ram. "Natural and synthetic chromenes, fused chromenes, and versatility of dihydrobenzo [h] chromenes in organic synthesis." Chemical reviews 114, no. 20 (2014): 10476-10526.
- 13. Halawa, Ahmed H., Mahmoud M. Elaasser, Ahmed M. El Kerdawy, Ahmed MAI Abd El-Hady, Hassein A. Emam, and Ahmed M. El-Agrody. "Anticancer activities, molecular docking and structure–activity relationship of novel synthesized 4 H-chromene, and 5 H-chromeno [2, 3-d] pyrimidine candidates." Medicinal Chemistry Research 26, no. 10 (2017): 2624-2638.
- 14. Dube, Pritam N., Nikhil S. Sakle, Sachin A. Dhawale, Shweta A. More, and Santosh N. Mokale. "Synthesis, biological investigation and docking study of novel chromen derivatives as anti-cancer agents." Anti-Cancer Agents in Medicinal Chemistry (Formerly Current Medicinal

- Chemistry-Anti-Cancer Agents) 19, no. 9 (2019): 1150-1160.
- 15. Aryapour, Hassan, Gholam Hossein Riazi, Shahin Ahmadian, Alireza Foroumadi, Majid Mahdavi, and Saeed Emami. "Induction of apoptosis through tubulin inhibition in human cancer cells by new chromene-based chalcones." Pharmaceutical biology 50, no. 12 (2012): 1551-1560.
- 16. Laxmikeshav, Kritika, Pooja Kumari, and Nagula Shankaraiah. "Expedition of sulfur-containing heterocyclic derivatives as cytotoxic agents in medicinal chemistry: A decade update." Medicinal Research Reviews 42, no. 1 (2022): 513-575.
- 17. Mohanty D, Rani MJ, Haque MA, Bakshi V, Jahangir MA, Imam SS, Gilani SJ. Preparation and evaluation of transdermal naproxen niosomes: formulation optimization to preclinical anti-inflammatory assessment on murine model. Journal of liposome research. 2020 Oct 1;30(4):377-87.
- 18. Ekladious, Iriny, Yolonda L. Colson, and Mark W. Grinstaff. "Polymer–drug conjugate therapeutics: advances, insights and prospects." Nature reviews Drug discovery 18, no. 4 (2019): 273-294.
- 19. Moloney, Cara, Fatemeh Mehradnia, Robert J. Cavanagh, Asmaa Ibrahim, Amanda K. Pearce, Alison A. Ritchie, Philip Clarke, Ruman Rahman, Anna M. Grabowska, and Cameron Alexander. "Chain-extension in hyperbranched polymers alters tissue distribution and cytotoxicity profiles in orthotopic models of triple negative breast cancers." Biomaterials Science 11, no. 19 (2023): 6545-6560.
- 20. Qiao, Yiting, Jianqin Wan, Liqian Zhou, Wen Ma, Yuanyuan Yang, Weixuan Luo, Zhiqiang Yu, and Hangxiang Wang. "Stimuli-responsive nanotherapeutics for precision drug delivery and cancer therapy." Wiley Interdisciplinary Reviews: Nanomedicine and Nanobiotechnology 11, no. 1 (2019): e1527.
- 21. Bin-Jumah M, Gilani SJ, Jahangir MA, Zafar A, Alshehri S, Yasir M, Kala C, Taleuzzaman M, Imam SS. Clarithromycin-loaded ocular chitosan nanoparticle: formulation, optimization, characterization, ocular irritation, and antimicrobial activity. International Journal of Nanomedicine. 2020 Oct 13:7861-75.
- 22. Jahangir MA, Anand C, Muheem A, Gilani SJ, Taleuzzaman M, Zafar A, Jafar M, Verma S, Barkat MA. Nano phytomedicine based delivery system for CNS disease. Current Drug Metabolism. 2020 Aug 1;21(9):661-73.
- 23. Mehradnia, Fatemeh, and Alexander Cameron.
 "The effect of Amine modification on siRNA delivery of redox-responsive PEGylated amphiphilic micellar nanoparticles for triple

- negative breast cancer therapy." British Journal of Pharmacy 7, no. 2 (2022): S1-S2.
- 24. Baghbani, Fatemeh, Mahdieh Chegeni, Fathollah Moztarzadeh, Samaneh Hadian-Ghazvini, and Majid Raz. "Novel ultrasound-responsive chitosan/perfluorohexane nanodroplets for imageguided smart delivery of an anticancer agent: Curcumin." Materials science and engineering: C 74 (2017): 186-193.
- 25. Hasaninejad, Alireza, Nooshin Golzar, Maryam Beyrati, Abdolkarim Zare, and Mohammad Mahdi Doroodmand. "Silica-bonded 5-n-propyloctahydro-pyrimido [1, 2-a] azepinium chloride (SB-DBU) Cl as a highly efficient, heterogeneous and recyclable silica-supported ionic liquid catalyst for the synthesis of benzo [b] pyran, bis (benzo [b] pyran) and spiro-pyran derivatives." Journal of Molecular Catalysis A: Chemical 372 (2013): 137-150.
- 26. Jiang, Xiaohong, Mingxing Ma, Mingjuan Li, Shihong Shao, Hong Yuan, Fuqiang Hu, Jianwen Liu, and Xuan Huang. "Preparation and evaluation of novel emodin-loaded stearic acid-g-chitosan oligosaccharide nanomicelles." Nanoscale research letters 15, no. 1 (2020): 93.
- 27. Muheem A, Jahangir MA, Jaiswal CP, Jafar M, Ahmad MZ, Ahmad J, Warsi MH. Recent patents, regulatory issues, and toxicity of nanoparticles in neuronal disorders. Current Drug Metabolism. 2021 Apr 1;22(4):263-79.
- 28. Mohr, Andreas, Peter Talbiersky, Hans-Gert Korth, Reiner Sustmann, Roland Boese, Dieter Bläser, and Heinz Rehage. "A new pyrene-based fluorescent probe for the determination of critical micelle concentrations." The journal of physical chemistry B 111, no. 45 (2007): 12985-12992.
- 29. Ansari MJ, Aldawsari MF, Zafar A, Soltani A, Yasir M, Jahangir MA, Taleuzzaman M, Erfani-Moghadam V, Daneshmandi L, Mahmoodi NO, Yahyazadeh A. In vitro release and cytotoxicity study of encapsulated sulfasalazine within LTSP micellar/liposomal and TSP micellar/niosomal nano-formulations. Alexandria Engineering Journal. 2022 Dec 1;61(12):9749-56.
- 30. Pan, Yuan-Jia, Yuan-Yuan Chen, Dong-Rui Wang, Chuan Wei, Jia Guo, Da-Ru Lu, Chih-Chang Chu, and Chang-Chun Wang. "Redox/pH dual stimuliresponsive biodegradable nanohydrogels with varying responses to dithiothreitol and glutathione for controlled drug release." Biomaterials 33, no. 27 (2012): 6570-6579.
- 31. Lee, Hee-Jeong, and Cheol-Hee Choi. "Characterization of SN38-resistant T47D breast cancer cell sublines overexpressing BCRP, MRP1,

- MRP2, MRP3, and MRP4." BMC cancer 22, no. 1 (2022): 446.
- 32. Baghbani, Fatemeh, Mahdieh Chegeni, Fathollah Moztarzadeh, Jamshid Aghazadeh Mohandesi, and Manijhe Mokhtari-Dizaji. "Ultrasonic nanotherapy of breast cancer using novel ultrasound-responsive alginate-shelled perfluorohexane nanodroplets: In vitro and in vivo evaluation." Materials Science and Engineering: C 77 (2017): 698-707.
- 33. Mohanty D, Zafar A, Jafar M, Upadhyay AK, Haque MA, Gupta JK, Bakshi V, Ghoneim MM, Alshehri S, Jahangir MA, Ansari MJ. Development, in-vitro characterization and preclinical evaluation of esomeprazole-encapsulated proniosomal formulation for the enhancement of anti-ulcer activity. Molecules. 2022 Apr 25;27(9):2748.
- 34. Baghbani, Fatemeh, and Fathollah Moztarzadeh. "Bypassing multidrug resistant ovarian cancer using ultrasound responsive doxorubicin/curcumin

- co-deliver alginate nanodroplets." Colloids and Surfaces B: Biointerfaces 153 (2017): 132-140.
- 35. Du, Yong-Zhong, Li-Li Cai, Jin Li, Meng-Dan Zhao, Feng-Ying Chen, Hong Yuan, and Fu-Qiang Hu. "Receptor-mediated gene delivery by folic acid-modified stearic acid-grafted chitosan micelles." International journal of nanomedicine (2011): 1559-1568.
- 36. Chatham, John C., Jianhua Zhang, and Adam R. Wende. "Role of O-linked N-acetylglucosamine protein modification in cellular (patho) physiology." Physiological reviews 101, no. 2 (2021): 427-493.
- Skovstrup, Søren, Signe Grann Hansen, Troels Skrydstrup, and Birgit Schiøtt. "Conformational flexibility of chitosan: a molecular modeling study." Biomacromolecules 11, no. 11 (2010): 3196-3207.

Copyright: ©2025 Golzar N. This article is distributed under the terms of the Creative Commons Attribution 4.0 International License [http://creativecommons.org/licenses/by/4.0/], which permits unrestricted use, distribution, and reproduction in any medium, provided you give appropriate credit to the original author[s] and the source, provide a link to the Creative Commons license, and indicate if changes were made.